Research Square

Preprints are preliminary reports that have not undergone peer review.
They should not be considered conclusive, used to inform clinical practice,
or referenced by the media as validated information.

Lithium Experimental Application Platform (LEAP) Part 1: Secondary-Containment Architecture and Downselection Framework for Flowing Liquid Lithium Fusion Systems

Yufan Xu

yxu@pppl.gov

Princeton Plasma Physics Laboratory

Yoichi Momozaki

Argonne National Laboratory

Michael Hvasta

Princeton Plasma Physics Laboratory

Robert Kaita

Princeton Plasma Physics Laboratory

Egemen Kolemen

Princeton University

Research Article

Keywords: Liquid Lithium, Secondary Containment, Plasma-Facing Components, Fusion Technology

Posted Date: July 27th, 2026

DOI: https://doi.org/10.21203/rs.3.rs-10103491/v1

License: This work is licensed under a Creative Commons Attribution 4.0 International License.
Read Full License

Additional Declarations: No competing interests reported.

Lithium Experimental Application Platform (LEAP) Part 1: Secondary-Containment Architecture and Downselection Framework for Flowing Liquid Lithium Fusion Systems

Yufan Xu[1*], Yoichi Momozaki[2], Michael Hvasta[1], Robert Kaita[1], Egemen Kolemen[1,3]

[1*]Princeton Plasma Physics Laboratory, 100 Stellarator Rd, Princeton, 08540, NJ, USA.
[2]Argonne National Laboratory, 9700 S Cass Ave, Lemont, 60439, IL, USA.
[3]Princeton University, Engineering Quadrangle, Princeton, 08540, NJ, USA.

*Corresponding author(s). E-mail(s): yxu@pppl.gov;

Abstract

Plasma-facing components (PFCs) that incorporate flowing liquid lithium surfaces are a promising technology because they can provide a renewable interface, modify recycling, support power exhaust, and potentially connect PFCs with fuel recovery. The deployment of liquid lithium PFC technology, however, is constrained by lithium chemical reactivity, fire and aerosol hazards, vacuum and inert gas operation, maintainability, and the need for rapid experimental iteration. Part 1 of this work develops a hazard-complexity metric for selecting secondary-containment architectures for flowing liquid-lithium systems. The framework is applied to six representative containment scenarios and to the Lithium Experimental Application Platform (LEAP), currently under construction at Princeton Plasma Physics Laboratory. LEAP uses a modular, room-sized argon glovebox as an inert secondary containment boundary for a staged flowing lithium program incorporating heating, diagnostics, magnetic field exposure, and future device interface capability. The analysis indicates that an inert, airtight secondary enclosure without scrubbers around an enclosed lithium loop provides a practical balance between hazard reduction and facility complexity for the present LEAP design requirements. This architecture offers a deployable

pathway for lithium PFC development and a transferable design logic for other reactive or conductive liquid metal systems.

Keywords: Liquid Lithium, Secondary Containment, Plasma-Facing Components, Fusion Technology

1 Introduction

1.1 Liquid lithium systems for fusion reactors

Liquid metals have high thermal and electrical conductivity and unique surface properties, making them desirable candidates for a wide range of applications in science and engineering (e.g., [1–3]). Liquid lithium, the lightest alkali metal ($Z = 3$), and lithium alloys are especially attractive for fusion science and technology because they have been proposed to address three key challenges at once: (i) self-replenishing plasma-facing components (PFCs) that survive extreme heat and particle fluxes, (ii) improved confinement via modified boundary conditions, and (iii) breeding, retention, transport, and recovery of fusion fuel species. There has been a decades-long interest in implementing liquid-metal plasma-facing components and liquid-metal fuel-cycle concepts for fusion devices [4–9] since the pioneering work by Golubchikov *et al.* (1996) [10] and subsequent experiments on Russian T-11 tokamak using liquid lithium capillary porous system (CPS) [11].

Flowing lithium used as a plasma-facing component offers a self-renewing interface: the exposed surface can be continuously replenished, which reduces cumulative damage from intense heat and particle fluxes. In contrast, a solid plasma-facing component presents a stationary near-surface region, and heat removal is ultimately constrained by conduction through the solid and by allowable surface temperatures set by melting, recrystallization, and thermomechanical limits. Without resurfacing, solid PFCs can also undergo self-amplifying degradation: leading edges, gaps, and tile/module misalignment concentrate the parallel heat flux and create localized hot spots. These overloads can drive cracking, recrystallization, and melting in solid divertor components, while the resulting surface deformation further worsens nonuniformity in heat flux [12–14]. Transient loads can also trigger crack growth and melt-layer motion or erosion, accelerating damage once overheating begins [15]. Arcing provides another localized erosion mechanism and can become more likely on damaged metal surfaces [16].

Unlike solid materials, liquid lithium can leverage forced convection as an added heat-removal mechanism, so heat-flux handling can be controlled by tailoring flow velocity, wetted geometry, and heat extraction. Several concept families have therefore been pursued, including divertorlets [17, 18], thin-film fast flows [19–21], capillary-porous systems with flow (CPSF) [22], LiMIT-style thermoelectric-MHD-driven surfaces [23], and lithium vapor-box divertors [24, 25]. These concepts span a broad design space for lithium-enabled power exhaust, including low-recycling flowing-surface approaches as well as vapor-shielded, high-recycling divertor regimes.

Experiments and simulations have demonstrated liquid-lithium PFC prototypes operating at incident heat fluxes of order $\sim 10\,\mathrm{MW/m^2}$ [18, 21, 26, 27] while avoiding excessive evaporation. Although so far the heat handling capabilities of these prototypes remain below the $\mathcal{O}(10^2)$ $\mathrm{MW/m^2}$ levels often projected for divertors in compact pilot-plant or reactor concepts (e.g., [28]), flowing lithium remains an attractive research direction. Ongoing experiments and near-term demonstrations are expected to clarify the achievable operating window and the key physics and engineering constraints that will determine its viability for reactor-relevant power exhaust [29].

Lithium's affinity for hydrogen isotopes lowers wall recycling, which can increase edge neutrals temperature, relax edge temperature gradients, and reduce the turbulence drive associated with temperature gradients from cold neutral returning from the wall [30]. This lithium-accessible low-recycling regime paved a new way for future fusion reactor designs and operations. Across devices such as CDX-U [30], LTX-β[31], NSTX/NSTX-U [32], FTU [33], TJ-II [34], HT-7 and EAST [35], lithium conditioning or lithium-based PFCs, such as limiters, have been associated with improved confinement, modified edge profiles, and, in some operating regimes, mitigation or suppression of ELM activity [36, 37].

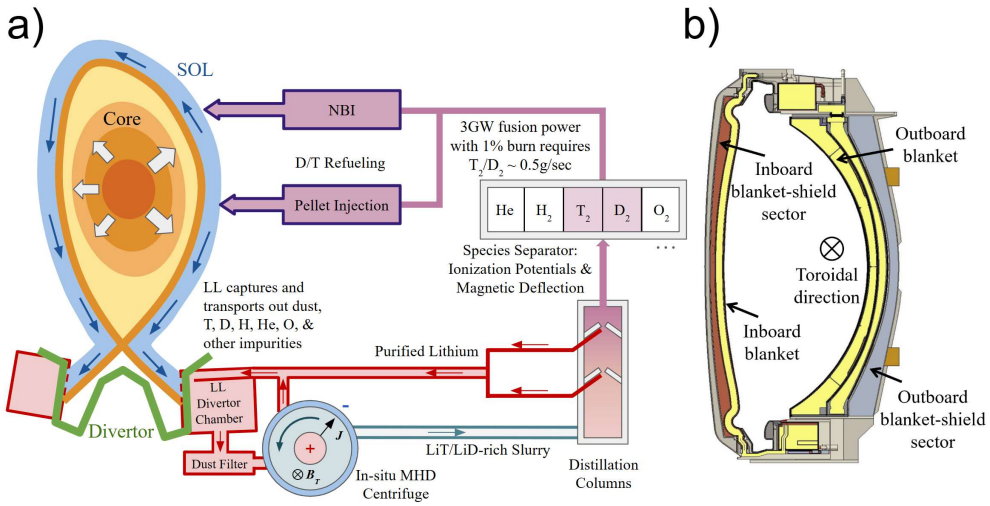


Fig. 1 Lithium systems in a fusion reactor. a) Schematics of a liquid lithium divertor with D/T extraction at the first wall. D/T enters the lithium divertor via a low-recycling regime, forming lithium deuteride, LiD, and lithium tritide, LiT. These lithium hydrides are further concentrated via an in-situ MHD centrifuge and transported to a distillation column system, where deuterium and tritium can be extracted and used as fuels. Figure adapted from Ono *et al.*, Nucl. Fusion (2017) [5], and de Castro *et al.*, Phys. Plasmas (2021) [7] b) Example of a fusion breeding blanket design. Figure adapted from the lead-lithium blanket design study of Spherical Tokamak Advanced Reactor (STAR) [38].

The deuterium/tritium (D/T) fuel cycle functions as the "circulatory system" of a fusion plant [39]. Tritium must be bred, extracted, processed, delivered to the

plasma, recovered from exhaust streams, and continuously recycled while maintaining rigorous accountancy and minimizing permeation losses. In most pilot-plant and reactor concepts, lithium-bearing blankets are the primary pathway to tritium self-sufficiency [38, 40, 41], which tightly couples blanket materials, tritium transport, and fuel-processing performance. In addition, tritium trapped in the first wall and divertor must be actively recovered and routed back into the fuel cycle, motivating flowing-liquid architectures that can provide both a low-recycling boundary and a controllable extraction pathway.

A further coupling arises because a lithium plasma-facing layer can itself become a significant tritium breeding region. In a three-dimensional neutronics study of an FNSF-like design with a 2.51 cm liquid-metal first wall, Bohm *et al.* (2019) [42] found that a lithium first wall increased the Tritium Breeding Ratio (TBR) by approximately 13% relative to the baseline when tritium produced in the lithium first wall was assumed to be recovered, but reduced the effective TBR by approximately 31% when that tritium was not recovered [42]. In that study, the lithium also reduced peak neutron-induced damage to the first wall and hydrogen/helium production relative to the baseline, indicating potential neutronics benefits beyond plasma-surface renewal. Nevertheless, the large sensitivity of TBR to first-wall tritium recovery means that reactor-relevant lithium PFCs must be treated as part of the fuel-cycle system, not only as heat-exhaust or wall-conditioning components. This strengthens the need for flowing-lithium test stands that can investigate intermediate questions of hydrogen-isotope transport, concentration, extraction, and recirculation in addition to MHD flow and plasma-facing performance.

Figure 1 a) illustrates a conceptual liquid-lithium divertor in which D/T species entering the divertor are absorbed into the lithium and converted into lithium hydrides, which are then removed from the plasma-facing region, concentrated (e.g., by an in-line MHD-based centrifuge), and processed in downstream systems such as distillation column systems to recover and re-inject deuterium and tritium into the fueling loop. Figure 1 b) shows a representative lead-lithium breeding blanket configuration in the design study of the Spherical Tokamak Advanced Reactor (STAR), highlighting that the blanket design, tritium breeding and extraction, and primary heat removal are inherently coupled at the system level.

Accordingly, the central question for liquid lithium systems in fusion is no longer whether they are scientifically compelling, but whether the remaining science and engineering gaps can be closed on timelines compatible with reactor and pilot-plant deployment, and whether they can be effectively integrated with existing fusion pilot-plant designs. The DOE Fusion Science and Technology Roadmap [9] identifies liquid metal plasma-facing components as a promising path for fusion power exhaust, but also makes clear that several gaps remain. These include free-surface and MHD flow stability, impurity control, lithium-material compatibility, heat transfer, component reliability, hydrogen isotope extraction, and D/T inventory management. Addressing these gaps requires more than isolated material tests. Flowing lithium systems must be operated at relevant temperatures, flow speeds, magnetic fields, and interface conditions so that transport, corrosion, impurity buildup, diagnostics, and recovery concepts can be evaluated together. Dedicated lithium and lithium-alloy test stands

are therefore needed to move from small component studies toward controlled flowing configurations, device-facing inserts, and eventually integrated liquid-metal core-edge and fuel-cycle platforms.

1.2 Legacy experience from alkali-metal fission systems

Large-scale liquid alkali-metal infrastructures have been developed primarily for liquid-metal-cooled nuclear fission reactor facilities [43]. The world's first breeder reactor prototype, the Experimental Breeder Reactor-I (EBR-I), was commissioned in 1951 [44] and used a sodium–potassium eutectic alloy (NaK) as the coolant. More recently, the Sodium-cooled Fast Reactor (SFR) has been pursued as a Generation IV reactor concept currently under development [45]. Alkali-metal coolants offer several advantages over current water-based reactors. Because sodium atoms are weak neutron moderators, fast-spectrum operation is facilitated, thereby enabling efficient transmutation and significantly reducing the production of transuranic waste [46]. The high boiling points of sodium and NaK yield large available temperature margins, increasing the permissible temperature rise in the coolant. High boiling points also allow the systems to operate at lower pressures. Consequently, liquid-metal-cooled systems can achieve higher thermodynamic efficiency than water-cooled systems, despite the lower specific heat capacities of liquid metals compared to water [47]. Sodium and NaK are also relatively abundant and exhibit favorable chemical compatibility with structural steels and many types of nuclear fuel cladding materials [48]. Nevertheless, the deployment of large-scale alkali-metal coolant systems presents significant challenges arising from the corrosive and highly reactive nature of these metals, as well as their propensity to leak. Therefore, rigorous design measures and specialized operational protocols are required to prevent, detect, and mitigate fires and other hazardous events [49]. This need is underscored by several historical incidents involving sodium fires, such as the sodium leak and subsequent fire at the Monju Nuclear Power Plant in 1995 [50]. Classical sodium and NaK handbooks [48, 49] provide valuable guidance for components, handling, and safety practice. International efforts to build fission systems cooled by liquid metals or molten salts have also invested extensively in safety and liquid-metal materials compatibility, driven in large part by the requirements of liquid-metal fast breeder reactors (LMFBRs), e.g., [51]. These lessons translate directly to fusion lithium facilities, which share many material and system-scale hazards.

1.3 Lithium-specific safety requirements

Development and implementation of liquid lithium systems at a reactor scale remains challenging. Lithium characteristics and risks have been discussed extensively in previous studies [7, 52]. Liquid lithium produces exothermic reactions with air and moisture. Lithium's reaction with water generates hydrogen, creating explosion risk. Lithium is also considered pyrophoric in powder form or liquid at elevated temperatures. The flowing lithium systems must address general alkali-metal safety requirements, such as leak prevention, inerting strategy for exclusion of air and moisture, hydrogen-generation risk, fire consequence management, contamination control, maintainability, and reliable operation during off-normal events. Moreover, any leak

or spill can generate corrosive and toxic aerosols and can mobilize radionuclides in tritium-containing lithium systems [52]. Past lithium loop incidents (e.g., [53, 54]) have already demonstrated credible leak and fire scenarios.

As a result, the design of liquid lithium systems should mainly focus on its containment strategy and minimizing the contact of non-compatible or reactive materials with lithium. Using IFMIF-DONES as a concrete design study, D'Ovidio *et al.* (2023) [52] presents a defense-in-depth fire protection strategy for large liquid-lithium facilities. A large-scale lithium system should implement robust primary confinement by mechanical codes and standards, minimization and segmentation of inventory where possible, room inertization (He/Ar) with gas monitoring, stainless-steel liners to prevent Li–concrete reactions, catch pans and drain and recovery systems, leak/smoke/flame detection, and compartmentalization isolation. A key conclusion is that for large lithium fires, fixed chemical-agent suppression may be unreliable, so passive measures (such as inerted rooms, spill capture and drainback, structural heat sinking, compartmentalization, etc.) are favored as the main line of defense, complemented by appropriately selected Class-D agents (e.g., Lith-X, Natrex-L, copper powder, carbon-based agents) and aerosol filtration strategies. Application of the MELCOR-fusion code has been demonstrated to analyze the transient accident associated with the lithium system for IFMIF-DONES test cell [55].

A series of regulatory standards for alkali-metal systems has been established. The International Building Code (section 307, 2021 edition) defines the maximum allowable quantities for a lithium system in a controlled area [56]. For example, the code limits storage and closed-container use to 22.68 kg of lithium per control area (this increases to 45.36 kg per control area when lithium is stored or used in a ventilated enclosure). The limit is 4.54 kg for open systems. A building may be permitted to have multiple control areas, up to four in total.

On fire protection, U.S. National Fire Protection Association Standard for Combustible Metals (NFPA 484) [57] covers facility design requirements, fire and explosion protection, powder, processing, machining, fabricating, finishing, storage, handling, etc., with applicable threshold masses. Other alkali metals fire protection standards can be found in The International Fire Code (IFC) [58], and the related defense-in-depth framework is covered in Fire Protection in Nuclear Power Plants (IAEA-TECDOC-1944) by the International Atomic Energy Agency (IAEA) [59]. It is strongly recommended, and in some cases required when the applicable NFPA 484 thresholds are met, to develop a fire protection plan and notify the local fire department, and make sure all personnel are trained to fight lithium fires.

Plumbing and piping system design under pressure and heating can refer to ASME B31.3, Process Piping Code [60], and ASME BPVC, the Boiler and Pressure Vessel Code [61], if applicable.

1.4 Risk-informed approach with infrastructure and operational complexity

It is sometimes neglected that safety systems that impose excessive procedural burden can increase operating cost and degrade overall safety by increasing the likelihood of human error. As outlined in human reliability analysis frameworks that have been

used in nuclear safety, task complexity and procedure quality are performance-shaping factors that increase estimated human error probability. As a consequence, designs that require extensive and highly complex operational procedures tend to be more error-prone [62].

These considerations motivate a fusion-oriented design framework that balances lithium safety requirements against infrastructure and operational complexity, enabling rapidly deployable research-scale flowing-lithium test stands. This need is most acute for platforms built for rapid iteration, where frequent hardware changes, evaluation of multiple PFC concepts, open-surface operation, strong magnetic fields, and eventual integration with a confinement device must all be accommodated on compressed development timelines. An integrated lithium platform, as a part of the technology development itself, should provide a stable safety boundary and standardized services that enable repeated test → modify → downselect cycles, while initiating a credible pathway toward integration of lithium systems and reactors.

In this study, we introduce a generalized design framework and secondary-containment choices for flowing liquid-lithium systems in fusion applications, with emphasis on safety, maintainability, and implementation in laboratory and industrial environments. Specifically, we present a reusable, risk-informed system engineering framework for selecting secondary-containment architectures for flowing liquid-lithium facilities and demonstrate the approach through the modular "gloveroom" concept used in the Lithium Experimental Application Platform (LEAP) at the Princeton Plasma Physics Laboratory (PPPL). The framework links mission requirements, including device-facing constraints, maintainability, prototyping flexibility, and facility readiness, to industrial safety and regulatory considerations. Although the present work centers on lithium, the design logic is intended to provide transferable engineering principles for a broader class of liquid metals and conductive fluids.

The paper is organized as follows. Section 2 introduces the hazard-complexity evaluation framework for lithium systems. Section 3 identifies a general downselect list of six secondary containment options. Section 4 presents the design requirements for flowing-lithium systems in LEAP and describes the selected modular secondary-containment architecture as an example. Section 5 discusses LEAP's interfacing strategy with fusion devices and considerations on the limitations of the gloveroom.

2 Methodology for determining containment architecture

There is no single secondary-containment solution that is optimal for every flowing lithium system. The appropriate design depends on the intended lithium inventory, operating modes, expected failure consequences, required flexibility for upgrades, and the degree of integration with facility infrastructure. For fusion applications, this trade space is especially important because the same platform must often support lithium safety, open-surface or vacuum interfaces, magnetic compatibility, maintainability, rapid experimental iteration, etc.

To make these tradeoffs explicit, we formulate a streamlined downselection metric for comparing candidate secondary-containment architectures in terms of two competing quantities: lithium hazard and facility complexity. Here, hazard represents the likelihood and consequence of lithium exposure to reactive environments, while facility complexity represents the infrastructure, controls, monitoring systems, and operational burden required to reduce that exposure. In general, additional safety features can lower the frequency or consequence of hazardous events, but they also increase hardware complexity, maintenance requirements, and procedural demands. Conversely, simpler systems may be easier to build and operate, but can leave fewer barriers between lithium and incompatible environments. The preferred architecture is therefore not necessarily the most elaborate one, but the one that provides sufficient hazard reduction without imposing unnecessary facility or operational complexity. In this work, the design metric is used as a comparative tool to identify that balance for research-scale flowing lithium systems.

2.1 Design Penalty Index

To compare candidate secondary-containment architectures on a common basis, we introduce a semi-quantitative *design penalty index*, $\mathcal{Q}$, that balances hazard reduction against system (infrastructure and operational) complexity. The index is intended as a comparative engineering tool for early-stage architecture downselection, not as a substitute for formal safety analysis, code compliance, or project-specific safety review. Lower values of $\mathcal{Q}$ correspond to more favorable overall designs. Table 1 summarizes the symbol definitions used in the metric.

Table 1 Definitions of symbols used in the hazard-complexity metric.

Symbol	Definition
$\mathcal{H}$	Hazard index [eq. (1)].
$\mathcal{C}$	Complexity index [eq. (1)].
$\mathcal{Q}$	Design penalty index [eq. (2)].
h_i	Impact score of hazard mode i.
c_j	Complexity score of safety feature j.
$p_i^{(\mathcal{H})}$	Exposure weighting for hazard mode i.
$p_j^{(\mathcal{C})}$	Requirement weighting for safety feature j.
α	Hazard weighting coefficient.
β	Complexity weighting coefficient.
γ_{eff}	Mitigation effectiveness [eq. (3)].
γ	Nominal mitigation effectiveness [eq. (4)].
k_H	Hazard sensitivity coefficient.
k_C	Complexity sensitivity coefficient.
x_m	Boolean of whether mitigation feature m is included.
η_m	Mitigation contribution of feature m.
$\mathbf{x}$	Selected mitigation features vector.
X	Set of acceptable design choices.

We define two main parameters, the intrinsic hazard and the complexity risks. The hazard index $\mathcal{H}$ represents the severity of the relevant lithium-specific failure consequences for a given system, such as reaction with air or moisture, aerosol generation, hydrogen production, radionuclide mobilization, and oxygen-deficiency hazards associated with inerting. The complexity index $\mathcal{C}$ represents the added facility and operational risk required by the containment concept, including enclosure requirements, atmosphere-control systems, detection systems, scrubbing or recovery systems, and the associated procedural and administrative burden. These indices represent risks that can be written as a sum of individual expectations based on Bernoulli's expected utility hypothesis for risk analysis [63],

$$\mathcal{H} = \sum_i p_i^{(\mathcal{H})} h_i, \qquad \mathcal{C} = \sum_j p_j^{(\mathcal{C})} c_j, \tag{1}$$

where $h_i \in [0, 5]$ represents the severity level or impact of each hazard mode in the lithium system, with 0 indicating negligible impact and 5 the highest impact and consequence. $c_j \in [0, 5]$ indicates the complexity impact associated with each safety feature, with 0 indicating negligible impact and 5 indicating the largest contribution to system complexity. In general, the higher c_j is, the more demanding, costly, and thus riskier it is to deploy a given feature. The corresponding weights $p_i^{(\mathcal{H})}$ and $p_j^{(\mathcal{C})}$ represent the probability of occurrence for each hazard mode and probability of implementing certain safety features, respectively.

We can further develop this from simple superposition to capture more nonlinear and intricate connections between hazards and complexity risks. It can be postulated that:

- Different designs are limited by various constraints and thus focus differently on hazards and complexity risks.
- A safety feature may become less effective when applied to a more hazardous system or when embedded in a more complex facility with more failure modes, interfaces, and operational dependencies.

These two conjectures lead to three coefficients: the hazard weighting coefficient, α; the complexity weighting coefficient β; and the mitigation effectiveness, γ_{eff}. The hazard weighting coefficient, $\alpha \in [0, 1]$, and the complexity weighting coefficient, $\beta \in [0, 1]$, define the practical design focus on addressing hazard and complexity risks. When $\alpha = 0$, the system design ignores the occurrence of any safety hazards, whereas facility complexity is not constrained at $\beta = 0$ (e.g., infinite budget and perfect graduate students). It should be noted that α and β should be determined relatively to reflect on the design interest, since $\mathcal{H}$ is not necessarily equal to $\mathcal{C}$. In addition, the mitigation effectiveness $\gamma_{\text{eff}} \in [0, 1]$ represents how effectively the selected safety architecture reduces the hazard in practice, where $\gamma_{\text{eff}} = 0$ corresponds to an ineffective safety feature and $\gamma_{\text{eff}} = 1$ corresponds to ideal, perfect hazard mitigation.

The design penalty index can be estimated as a simple mathematical model to qualitatively capture the basic interplay between the risks,

$$\mathcal{Q} = \alpha\mathcal{H}\left(1 - \gamma_{\text{eff}}\right) + \beta\mathcal{C}, \tag{2}$$

where the first term represents the residual hazard penalty after accounting for the effectiveness of the safety architecture, while the second term represents the direct penalty associated with system complexity. For fixed mitigation effectiveness, this form gives the desired behavior: $\mathcal{Q}$ increases with larger hazard and greater complexity, and decreases as mitigation effectiveness improves.

The definition of mitigation effectiveness is less certain. In many cases, we can simply assume $\gamma = 1$ if mitigation effectiveness is included, or 0 if it can be ignored. However, because practical effectiveness may degrade as the intrinsic hazard and system complexity increase, we can choose to model an effective mitigation coefficient as a function of $\mathcal{H}$ and $\mathcal{C}$,

$$\gamma_{\text{eff}} = \gamma \exp\left(-k_H\mathcal{H} - k_C\mathcal{C}\right), \tag{3}$$

where $k_H > 0$ and $k_C > 0$ are hazard and complexity sensitivity coefficients selected by users, respectively. The exponential form ensures $0 < \gamma_{\text{eff}} \leq \gamma$. The nominal mitigation effectiveness γ can itself be constructed from the selected safety features. For example, a binary $x_m \in \{0, 1\}$ denotes the presence or absence of mitigation feature m, such as inerted secondary containment, atmosphere monitoring, drainback, spill capture, or aerosol filtration, then

$$\gamma = 1 - \exp\left(-\sum_m \eta_m x_m\right), \tag{4}$$

where η_m is the contribution of feature m to the overall mitigation effectiveness. This representation ensures that γ remains bounded between 0 and 1, so that $0 \leq \gamma_{\text{eff}} \leq 1$, while also capturing diminishing returns as more safety features are added.

The residual hazard term in eq. (2) can also be interpreted from a reliability perspective. In a full component-level treatment, a hazard contributes to the residual hazard penalty only when the primary hazard containment fails and the relevant safety layers also fail during the operating period. Such a treatment could be constructed from component mean-time-between-failure data and the assumed safety-layer structure. However, those data are generally unavailable during early-stage facility design, and the resulting model would introduce many system-specific parameters. The present study therefore uses the compact hazard-complexity form in eq. (2) as a comparative downselection metric, while Appendix A gives a reliability-based interpretation of the mitigation term.

The optimal secondary-containment concept is then obtained by minimizing $\mathcal{Q}$ over the set of acceptable design choices $\mathbf{x} \equiv (x_1, x_2, x_3, ...) \in X$,

$$\mathbf{x}^* = \arg\min_{\mathbf{x}\in X} \mathcal{Q}(\mathbf{x}), \tag{5}$$

subject to any additional project-specific constraints, such as lithium inventory, open-surface operation, magnetic-field compatibility, vacuum interfaces, available building

infrastructure, or code-related requirements. This optimization also allows investigation of the optimal continuous design features (e.g., argon purge rate, oxygen and moisture set point, spill-capture capacity, and redundancy level) to understand which features are most valuable when added safety begins to have diminishing returns and how strongly complexity penalizes further mitigation.

i	Hazards	h_i	Justification
1	H_2 generation with bulk water	5	Large quantity of hydrogen gas can be generated in a short time. Explosion risk.
2	H_2 generation with air moisture	4	Accumulation of hydrogen over time. Explosion risk.
3	Lithium Fire with O_2	3	Exothermic reaction. Oxide also reacts with water to form hydroxide.
4	Lithium Fire with N_2	2	Mild exothermic reaction. Can generate toxic ammonia gas with moisture and O_2.
5	Lithium aerosol/smoke	3	Reduce visibility, toxic, radionuclides mobilization. Indication of fire.
6	Asphyxiation by inert gas	1	Inert containment hazard, can be mitigated through monitoring and control, not common.

Table 2 List of hazards and their impact, h_i, in a generic lithium system. These hazards will be considered in the analysis of this study.

j	Safety Feature	c_j	Justification
1	Watertight 2nd containment	2	Relatively low complexity. Simple waterproof material and design.
2	Airtight 2nd containment	3	Medium complexity. Airtight seal or vacuum system are often available off-the-shelf. Requires maintenance and leak check.
3	Wet scrubber	5	Very complex and less common. Difficult to build and maintain. Needs dedicated water supply and waste drain.
4	Dry scrubber (O_2/N_2)	4	Requires maintenance. Need to replace filter/scrubber and add exhaust. Expensive.
5	Ventilation & exhaust	3	Medium complexity. Emergency exhaust to avoid aerosol and hydrogen accumulation.
6	Dehumidifier	2	Commercial product available. Requires additional maintenance.
7	H_2 detector	1	Low impact. Easy to deploy.
8	H_2O/O_2/N_2 analyzer	1	Low impact. Easy to deploy.

Table 3 List of safety features and their impact, c_j, on complexity in a generic lithium system. These safety features will be considered in the analysis of this study.

In the present study, this minimization is evaluated over a finite set of representative containment architectures rather than solved as a continuous optimization problem. A detailed derivation of the optimization problem in eq. (5) is shown in Appendix B.

The design penalty index provides a transparent basis for comparing containment strategies, identifying the dominant safety drivers, while balancing risk reduction against implementation burden. This risk-informed matrix can be adapted to different classes of alkali-metal systems simply by changing the modes, their impacts, and probabilities. In the present work, this theoretical framework is used as a structured downselection method for representative containment scenarios and to support the modular inerted secondary-containment architecture adopted for LEAP.

2.2 Simplified parameters

The probability and severity of lithium-related hazards are difficult to quantify precisely and are strongly dependent on the specific system configuration. For an initial evaluation of secondary-containment concepts, we therefore adopt a simplified and conservative assumption: the comparison is conditioned on a primary-containment breach for all candidate designs, and therefore a secondary containment is required by definition. Under this condition, the primary containment itself is not used to distinguish between architectures. Instead, the comparison focuses on how the selected secondary-containment concept modifies the operator or facility exposure to the resulting hazards. For example, hydrogen generation from moisture is more likely if leaked lithium is exposed to ambient air than if the same leak occurs within an inert-gas-filled secondary enclosure, even when both systems use highly reliable primary containment. This simplification allows the design matrix to isolate the safety value of the secondary-containment architecture itself.

The impact of the hazards h_i, and the impact on the complexity risk c_j, are both assumed to be generic and independent of the design. For simplicity, discrete, nonzero integers are used so that $h_i,\ c_j \in \{1, 2, 3, 4, 5\}$ in ascending order of impact. Table 2 shows common lithium system related hazards with justification that have been included in the analysis for this study and table 3 shows a list of common safety features used in lithium systems and their impact on complexity with justification that has been considered in this study. Furthermore, $p_i^{(\mathcal{H})}$ is defined as

$$p_i^{(\mathcal{H})} = \begin{cases} 1 & \text{full exposure upon failure} \\ 0.5 & \text{possible exposure to hazard but under control} \\ 0 & \text{no exposure to hazard} \end{cases} \tag{6}$$

This assumes the scenario that primary containment has failed. Here, "under control" means any lithium escaped from the primary containment is under automatic facility control so no or little manual operation is required. Similarly,

$$p_j^{(\mathcal{C})} = \begin{cases} 1 & \text{if feature is needed} \\ 0.5 & \text{if feature is optional} \\ 0 & \text{if feature is not needed} \end{cases} \tag{7}$$

Therefore, the probability of having a certain feature has been effectively translated to whether this feature is needed in the system. For instance, an essential feature has a 100% probability of showing up in the system.

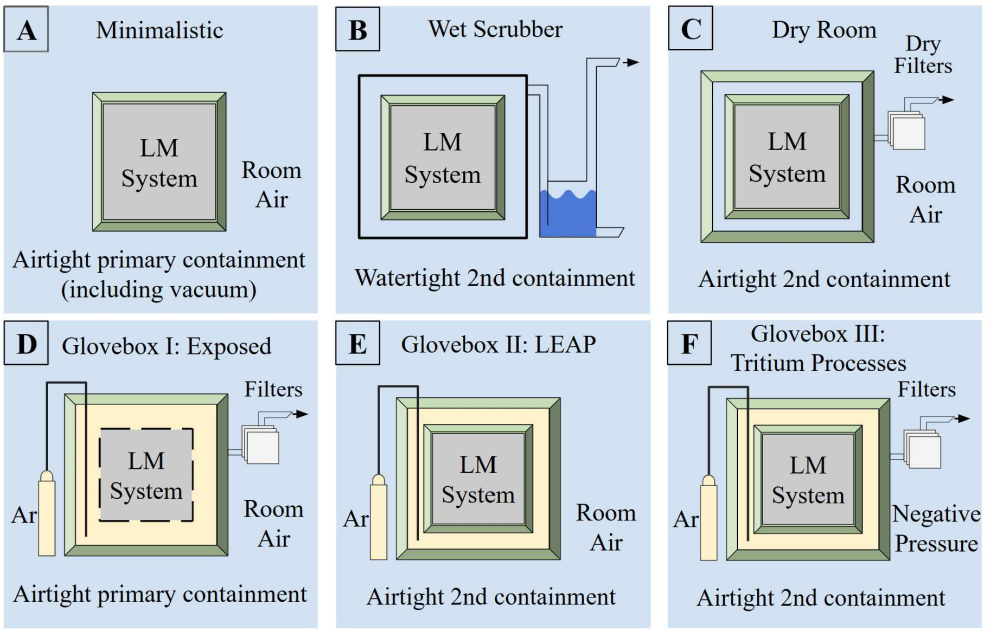


Fig. 2 Six scenarios for the liquid metal containment systems. (A) A minimalistic setup: a primary containment for liquid lithium. (B) A watertight or semi-airtight secondary containment encloses the airtight primary containment and is also connected to a wet scrubber. (C) A typical dry room: a humidity-controlled secondary containment is connected to a dehumidifier or a dry filter system. (D) A glovebox with open-surface liquid metal: airtight primary containment is filled with inert gas and connected to a dry filter system. (E) A basic glovebox setup: airtight secondary containment is filled and purged with inert gas, such as argon, but does not connect to any filters or scrubbers. (F) A fully equipped glovebox with oxygen, humidity, and/or nitrogen filter and scrubbers. Negative pressure is implemented for containing radionuclides.

3 Lithium system scenarios and requirements

We can summarize existing lithium containment systems into six general example scenarios, as shown in the six panels of fig. 2. These six scenarios do not exhaust all the options for developing lithium systems. They are treated as representative cases that have been used in the downselect for this study. Each scenario corresponds to a unique set of $p_i^{(\mathcal{H})}$ and $p_j^{(\mathcal{C})}$.

Scenario A (Minimalistic) setup is shown in fig. 2 (A). Liquid lithium is contained inside an airtight primary containment, usually filled with inert gas, such as argon, or under vacuum for free-surface operations. There is essentially only one barrier between

liquid lithium and the room environment. This is the simplest approach for various tabletop lithium systems with a limited amount of lithium, and therefore has a low complexity risk. However, it is the least safe option because the leaked lithium would have direct exposure to the exterior environment with oxygen, nitrogen, moisture and even possibly bulk water in case of failure. Table 4 reflects that scenario A is under exposure to hydrogen generation via moisture, lithium fire, and smoke. Hydrogen generation with bulk water can be limited by facility controls, such as excluding nearby water sources or using dry or pre-action sprinkler systems. Nevertheless, scenario A needs the least amount of safety features (hydrogen detector and ventilation) and hence has the lowest complexity risk among all scenarios, as shown in table 5.

Scenario B (Wet scrubber) shown in fig. 2 (B) is a uniquely designed secondary containment (which can be an enclosure or a building) that connects to a wet scrubber system. In case of a liquid metal fire, the generated gas and smoke can be directed to a water container for reaction and passivation (e.g., the METL sodium system at Argonne National Laboratory). The wet scrubber does not completely mitigate the fire and hydrogen hazards, but has been implemented as a control method to constrain the consequences of a lithium incident. Scenario B in table 4 lists most of the hazards as under control, $p_i^{(\mathcal{H})} = 0.5$. Because there is a watertight secondary containment, it is unlikely lithium will see any bulk water to generate hydrogen, $p_1^{(\mathcal{H})} = 0$. However, wet scrubbers are less common in lithium processing, and they are difficult to build and maintain. They also require dedicated water supplies and waste drains that are isolated from lithium usage. Therefore, we consider that wet scrubber has the highest complexity risk impact among all the safety features (table 3).

Scenario C (Dry room) shown in fig. 2 (C) is a humidity-controlled only setup with airtight secondary containment. These dry-room scenarios are commonly adopted in lithium battery production. Therefore, there is no moisture or bulk water, and hydrogen generation upon failure can be eliminated. Therefore, a hydrogen detector is optional. Lowering the moisture in the secondary containment also lowers the reaction speed of oxygen and nitrogen with lithium. However, exposed lithium can still ignite and react with oxygen and nitrogen in the air at a high temperature. Therefore, $p_i^{(\mathcal{H})} = 0.5$ for fire and smoke, as shown in table 4.

Scenario D (Glovebox I) shown in fig. 2 (D) is a glovebox setup with dry filters and an open lithium surface. It is similar to Scenario A, except that an airtight containment is filled and purged with argon gas. Argon purge and filtration will maintain low levels of oxygen, humidity, and nitrogen, often at $\sim$ 1 ppm or lower, to minimize lithium reaction with air inside the glovebox. This glovebox is essentially just an atmosphere-controlled primary containment under near-room pressure. This is often considered safe for a small amount of lithium (grams) operation. However, due to the lack of secondary containment, $p_i^{(\mathcal{H})} = 0.5$ for all hazards. Because the enclosure is inerted with argon, oxygen monitoring is required to manage oxygen-deficiency hazards.

Scenario E (Glovebox II) shown in fig. 2 (E) is a simple glovebox or enclosure with reduced functionalities: airtight secondary containment around an enclosed primary containment, and is filled and purged with inert gas, such as argon. This setup does not connect to any filters or scrubbers, and generally can reach $\lesssim$ 1000 ppm of oxygen, humidity, and nitrogen by purging, sufficient for secondary containment to suppress

Table 4 Hazard index, $\mathcal{H}$, and qualitative level of exposure to hazards, $p_i^{(\mathcal{H})}$ for each scenario (A to F). The value is estimated according to eq. (6). Here, $p_i^{(\mathcal{H})} = 0$ means low probability of exposure to hazards after failure of primary containment, $p_i^{(\mathcal{H})} = 0.5$ means possible exposure to hazards but under some level of automatic control, and $p_i^{(\mathcal{H})} = 1$ means full exposure or high probability of hazard to occur upon failure of the primary containment. The impact h_i is taken from table 2.

i	Hazards	h_i	$p_i^{(\mathcal{H})}$					
			A	B	C	D	E	F
1	H2 (bulk H2O)	5	0.5	0	0	0.5	0	0
2	H2 (moisture)	4	1	0.5	0	0.5	0	0
3	Li Fire (O2)	3	1	0.5	0.5	0.5	0	0
4	Li Fire (N2)	2	1	0.5	0.5	0.5	0	0
5	Li Smoke (fire)	3	1	0.5	0.5	0.5	0	0
6	Asphyxiation	1	0	0	0	0.5	0.5	0.5
	Hazard index, $\mathcal{H}$		14.5	6	4	9	0.5	0.5

and eliminate fire or hydrogen generation. Because the enclosure is inerted with argon, it also introduces a controlled asphyxiation hazard from a leak in the glovebox.

Scenario F (Glovebox III) shown in fig. 2 (F) is a fully-equipped glovebox or enclosure with oxygen, humidity, and nitrogen scrubbers. The primary or secondary containment can be enclosed by a negative pressure to avoid any radioactive breach if it is involved. This also provides additional margin for overpressure [52]. There is no exposure to hazards even if the primary containment is breached. However, scenario F requires most of the safety features and thus has the highest complexity index, as shown in table 5.

Table 5 Complexity index, $\mathcal{C}$, and qualitative level of feature requirement, $p_j^{(\mathcal{C})}$ for each scenario (A to F). The value is estimated according to eq. (7), in which $p_j^{(\mathcal{C})} = 0$ means the feature is not needed for the setup, hence zero probability of appearance in the system. $p_j^{(\mathcal{C})} = 0.5$ means optional and $p_j^{(\mathcal{C})} = 1$ means necessary and crucial for the confinement. The impact c_j is taken from table 3.

j	Safety feature	c_j	$p_j^{(\mathcal{C})}$					
			A	B	C	D	E	F
1	Watertight 2nd containment	2	0	1	0	0	0	0
2	Airtight 2nd containment	3	0	0	1	1	1	1
3	Wet scrubber	5	0	1	0	0	0	0
4	Dry scrubber (O_2/N_2)	4	0	0	0	1	0	1
5	Ventilation & exhaust	3	1	1	1	1	1	1
6	Dehumidifier	2	0	0	1	0.5	0	1
7	H_2 detector	1	1	1	0.5	0.5	1	0.5
8	H_2O/O_2/N_2 analyzer	1	0	0	1	1	1	1
	Complexity index, $\mathcal{C}$		4	11	9.5	12.5	8	13.5

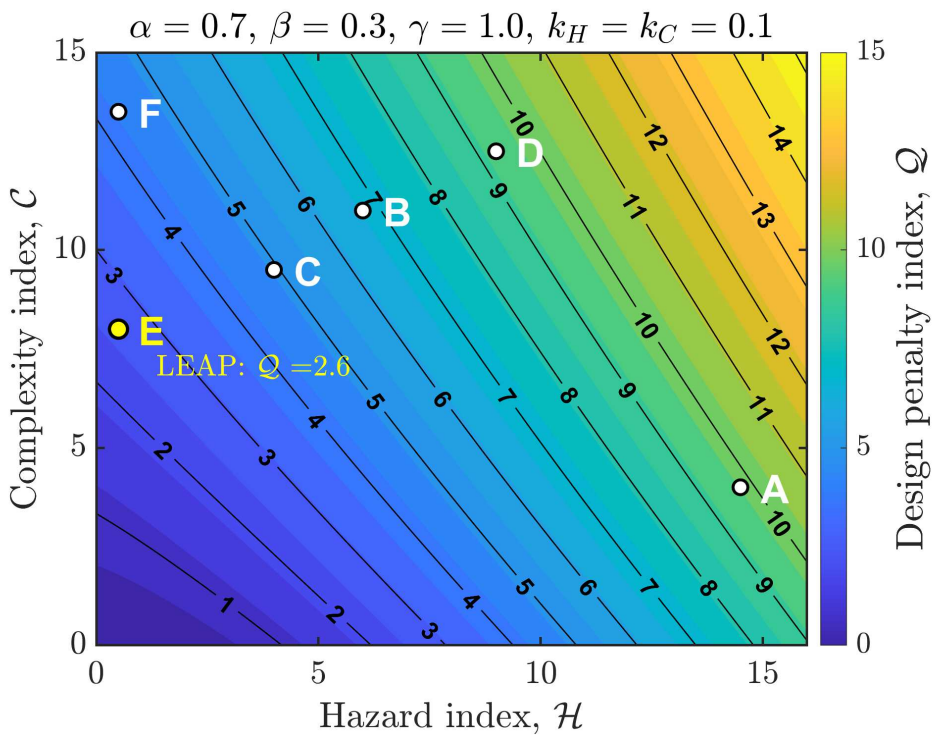


Fig. 3 Design penalty index $\mathcal{Q}$ map for the six representative secondary containment scenarios. The contour shows $\mathcal{Q} = \alpha\mathcal{H}(1 - \gamma_{\text{eff}}) + \beta\mathcal{C}$ with $\gamma_{\text{eff}} = \gamma \exp(-k_H\mathcal{H} - k_C\mathcal{C})$, using $\alpha = 0.7$, $\beta = 0.3$, $\gamma = 1.0$, and $k_H = k_C = 0.1$. Points A–F correspond to the six containment scenarios based on existing liquid lithium systems listed in fig. 2. Scenario E, corresponding to the LEAP gloveroom architecture, gives the lowest penalty index, $\mathcal{Q} \approx 2.6$, indicating a favorable balance between reduced lithium hazard exposure and moderate facility complexity.

4 Lithium Experimental Application Platform (LEAP)

4.1 Gloveroom containment solution

We present the Lithium Experimental Application Platform (LEAP), currently under construction at Princeton Plasma Physics Laboratory, as a case study. LEAP is a modular, argon-inert liquid lithium test platform for flowing lithium PFC development, diagnostic validation, safety architecture evaluation, and future device integration studies. The initial system is designed for a lithium inventory of 22.68 kg (50 lb), remaining below the IBC's maximum allowable quantity of 45.36 kg (100 lb) for a control area using a ventilated enclosure.

Figure 3 summarizes the tradeoff between hazard reduction and implementation complexity for the six representative containment scenarios under the PPPL design

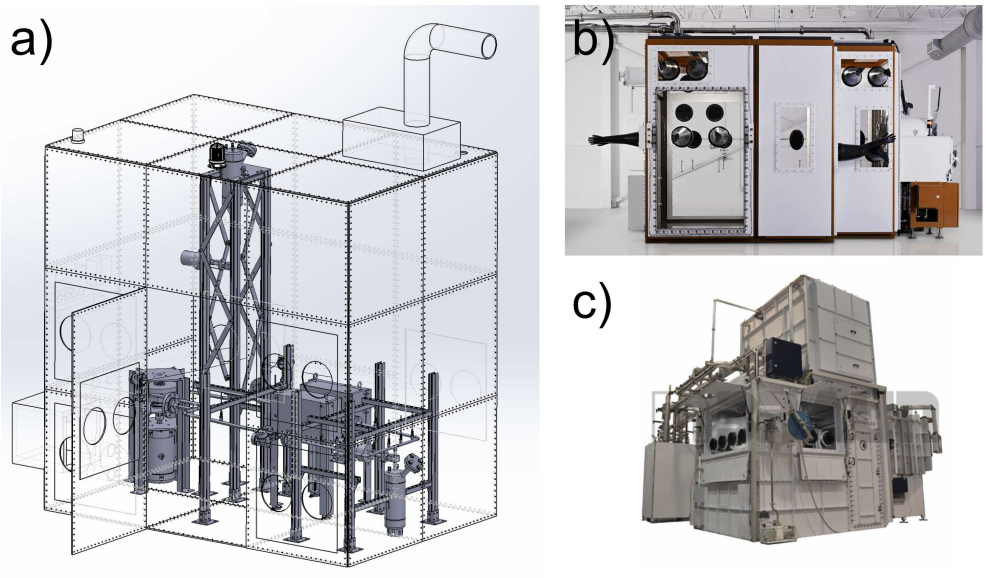


Fig. 4 (a) A model of LEAP gloveroom with a Phase I liquid lithium loop inside. (b) Example product of a customized atmosphere-controlled enclosure. Courtesy of Inert Corp. (c) Another example product. Courtesy of M.Braun Inc.

preference used in this study. This example uses safety-prioritized weighting parameters, with $\alpha = 0.7$, $\beta = 0.3$, $\gamma = 1.0$, and $k_H = k_C = 0.1$. The contour field shows that the design penalty index $\mathcal{Q}$ increases with both hazard index $\mathcal{H}$ and complexity index $\mathcal{C}$, with a nonlinear contribution from the degradation of the effective mitigation coefficient. Scenario A is penalized by its high residual hazard despite its low complexity, whereas Scenarios B, C, D, and F reduce selected hazards by adding more infrastructure and operational controls. Scenario E, corresponding to the LEAP gloveroom architecture, lies in the low-hazard, moderate-complexity region and gives the lowest penalty value, $\mathcal{Q} \approx 2.6$. Under the present design priorities, this supports the selection of an inert, airtight secondary enclosure around an enclosed lithium loop for research-scale flowing lithium systems.

The ranking in Figure 3 should be interpreted as a design-specific downselection result rather than a universal ordering of containment strategies. Different facilities may assign different values to α, β, γ, k_H, and k_C depending on lithium inventory, open-surface operations, tritium relevance, available infrastructure, staffing, and regulatory constraints. For example, a tritium processing system may justify the added complexity of Scenario F, whereas a small gram-scale lithium experiment may accept a simpler architecture. The value of the framework is that these priorities can be made explicit and varied systematically, allowing the preferred containment architecture to follow the mission requirements rather than being prescribed *a priori*.

The defining feature of LEAP is a room-scale, prefabricated glovebox that serves as the secondary containment boundary ($3.93\,\mathrm{m}\ L \times 2.37\,\mathrm{m}\ W \times 3.35\,\mathrm{m}\ H$). As shown

in fig. 4 (a), it is a commercially fabricated, fully customized, walk-in argon enclosure that houses the lithium loop while maintaining a continuously purged and monitored inert atmosphere during operation, with target oxygen, nitrogen, and moisture levels below 1000 ppm. Figure 4 (b) and (c) show two examples of the modularized gloverooms used for additive manufacturing, nuclear, or pharmaceutical applications. The enclosure is sized to support lithium experiments with a high-field magnet, with fully customized interface panels for gas, vacuum, electrical, cooling, and diagnostic feedthroughs, as well as future connections to external vacuum vessels. Active circulation inside the enclosure improves gas mixing, temperature uniformity, and analyzer response, while monitoring of oxygen, moisture, temperature, and hydrogen provides operational awareness during both inert operation and access conditions. The gloveroom also integrates facility-level functions that are difficult to achieve with a conventional glovebox, including door access with oxygen threshold interlocks, active HVAC (6.59 kW, or 22 500 BTU/hr), viewing ports, HEPA filtration, and anchor points and support structures for the liquid lithium and magnetic field systems. The enclosure and loop interfaces have completed PPPL design review processes, providing a traceable design basis for lithium operation in a national laboratory environment. In this sense, the LEAP gloveroom is not only a protective enclosure but also a standardized experimental infrastructure that combines inert secondary containment, modular utility access, and device-integration capability for iterative, flowing lithium PFC development.

A phased development strategy is used for the LEAP flowing lithium loop, with each stage increasing the level of physics integration and operational complexity. Phase I is an enclosed loop containing 2.27 kg (5 lb) of lithium, with a test section passing through a uniform magnetic field of up to 0.5 T. This phase will characterize the pressure and flow performance of the moving magnet pump, validate thermometry and velocimetry diagnostics, and demonstrate lithium flow at up to 16 GPM (1 L/s) under strong magnetic field conditions relevant to flowing lithium PFC and hydrogenic fuel transport concepts [5].

Phase II extends LEAP to porous or open-surface lithium flow with applied heating and magnetic field exposure, using inventories up to 22.68 kg (50 lb). This phase will require modifications to the piping and support structure to accommodate PFC-relevant test articles. The primary goal is to characterize open-surface liquid lithium PFC performance under combined thermal loading and magnetic field conditions, including MHD pressure drop, heat transfer scaling, surface stability, and lithium-induced erosion or compatibility effects.

Phase III will develop interface strategies between LEAP and existing fusion devices, such as NSTX-U, to enable a continuous flowing lithium PFC loop coupled to a divertor surface. This stage is intended to move from standalone loop validation toward device-integrated operation, where lithium delivery, recovery, diagnostics, safety controls, and secondary containment must operate as a coordinated system.

Table 6 Representative numerical inputs used to evaluate the LEAP gloveroom architecture in the design penalty framework. LEAP is treated as Scenario E in tables 4 and 5. The values are semi-quantitative estimates intended for comparative downselection rather than probabilistic risk assessment.

Symbol	LEAP value	Basis
α	0.7	User-defined safety-prioritized weighting.
β	0.3	User-defined complexity weighting.
$\mathcal{H}$	0.5	Hazard index for Scenario E, calculated from table 4.
$\mathcal{C}$	8.0	Complexity index for Scenario E, calculated from table 5.
γ	1.0	Nominal mitigation effectiveness is included.
k_H	0.1	Representative hazard sensitivity of effectiveness.
k_C	0.1	Representative complexity sensitivity of effectiveness.
γ_{eff}	0.4	Mitigation effectiveness calculated from eq. (3).
$\mathcal{Q}$	2.6	Design penalty index calculated from eq. (2).

5 Discussion

5.1 Integration of LEAP with fusion devices

The LEAP architecture by itself should be distinguished from plant-scale blanket loops and full fuel-cycle test facilities. LEAP is designed as a research-scale, modular secondary-containment platform for flowing lithium PFC development, diagnostic validation, MHD flow studies, safety architecture evaluation, and future device-interface concepts. It is therefore not intended to replace industrial-scale blanket or tritium fuel-cycle facilities, such as integrated lithium-lead and fuel-cycle test systems being developed for plant-relevant blanket and tritium-processing demonstrations. At larger plant scale, other containment strategies, including double-wall piping, leak-before-break design philosophy, guard vessels, segmented drain tanks, inerted pipe chases, and dedicated tritium confinement systems, may be more appropriate than a room-scale gloveroom. The value of LEAP is instead to provide a flexible intermediate platform and vacuum interface where lithium PFC concepts, flow control, diagnostics, hydrogen-isotope uptake and recovery concepts, and confinement-device interfaces can be developed before translation to larger blanket or fuel-cycle infrastructure.

The National Spherical Torus Experiment-Upgrade (NSTX-U) at the Princeton Plasma Physics Laboratory has features that are useful for a practical demonstration of integrating LEAP into a fusion device. The NSTX-U machine is equipped with 15 MW of neutral beam injection (NBI) and 6 MW of ion cyclotron resonance heating (ICRH), which can provide high heat loads to the divertor.

Because NSTX-U is a spherical tokamak, the surface area of the divertor is relatively small compared with those of large aspect ratio tokamaks with similar plasma heating capabilities. This practical advantage was demonstrated with the liquid lithium divertor (LLD) in NSTX. The NSTX device was the predecessor of NSTX-U and had the same divertor surface area.

The LLD was located on the outboard divertor as shown in fig. 5. It consisted of four segments with a radial width of 22 cm, separated by a row of graphite tiles that included a radial array of Langmuir probes for measurements at the divertor

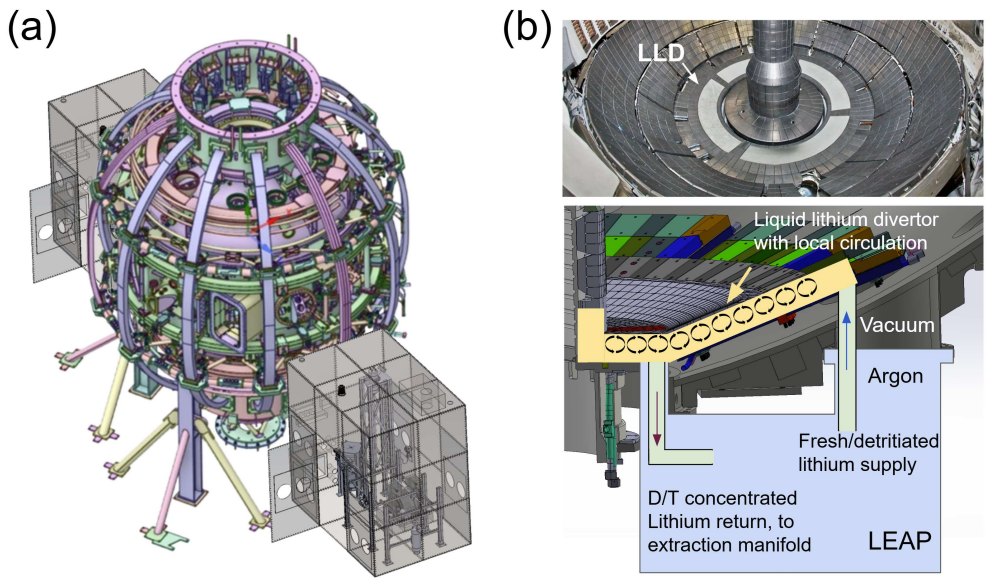


Fig. 5 (a) Conceptual drawing with two LEAP gloverooms around the vacuum vessel in NSTX-U Test Cell. The exterior structure of the modular gloveroom can be modified to save space. Location of the gloverooms is arbitrarily chosen for illustration purposes only. (b) Conceptual LEAP interface with NSTX-U. LEAP enables a flexible interfacing by argon-to-vacuum feedthroughs with flange connections to the interior of NSTX-U's lower divertor region, where LLD segments were placed. Photo of LLD is adapted from H. Kugel *et al.*, Fus. Eng. Design (2012) [32]. Liquid lithium divertor is coupled to a supply/drain system contained in LEAP's gloveroom system. Even though no tritium operation is planned for NSTX-U, the return loop can be used for pumping deuterium and tritium to the extraction manifold in Fusion Power Plants (FPPs) with a similar method. The cleaned lithium will re-enter the supply line.

strike points. There was also a toroidal gap that electrically isolated the inboard and outboard divertors. Each LLD segment consisted of a 0.25 mm stainless steel sheet that was dynamically bonded to a 2.2 cm thick copper substrate. A 0.17 mm layer of molybdenum was plasma-sprayed onto the stainless steel. This formed a surface with 45% porosity for retaining static liquid lithium, which was kept liquefied with heaters in the copper substrate.

The LEAP system is intended to provide flowing liquid lithium from the outboard edge of the outboard divertor to the toroidal gap. Because the LEAP gloverooms are modular, their number around the NSTX-U vacuum vessel can be adjusted to meet lithium inventory, pumping power, and flow required by any flowing liquid lithium divertor design. A possible configuration for the LEAP gloverooms in the NSTX-U Test Cell and a conceptual interface with the vacuum vessel are shown in fig. 5.

The modularity of the LEAP system is itself a safety feature. Each LEAP gloveroom are expected to accommodate only their individual lithium inventories. In that way, no component has to meet the safe handling requirements for the entire lithium inventory. Each LEAP gloveroom also feeds liquid lithium into a common manifold

inside NSTX-U vacuum vessel. This redundancy allows NSTX-U to be provided with liquid lithium if any LEAP gloveroom becomes inoperable.

5.2 Limitations and considerations of the LEAP lithium loop and gloveroom

The LEAP gloveroom provides a practical secondary containment solution for flowing lithium experiments, but its room-scale argon enclosure also introduces operational limitations. The most important are purge time and argon consumption. For a conventional sweep-through purging, the required inert-gas volume can be estimated from the complete-mixing relation $\dot{V}t = V\ln(C_0/C_t)$, with a correction factor K used to account for nonideal mixing [64]. $K = 1$ is perfect mixing. The argon purge time is

$$t = \frac{V}{K\dot{V}} \ln\left(\frac{C_0}{C_t}\right), \tag{8}$$

where V is the enclosure volume, $\dot{V}$ is the argon purge rate, C_0 is the initial oxygen concentration, and C_t is the target concentration. For $V \approx 12\,\mathrm{m}^3$ ($424\,\mathrm{ft}^3$), $\dot{V} = 10\,\mathrm{scfm}$, $C_0 = 210\,000\,\mathrm{ppm}$, and $C_t = 1000\,\mathrm{ppm}$, the ideal complete-mixing estimate gives $t \approx 3.8\,\mathrm{h}$ and $\sim 2300\,\mathrm{scf}$ of argon. With a mixing correction factor of $K = 0.5$, the estimate increases to $t \approx 7.6\,\mathrm{h}$ and $\sim 4500\,\mathrm{scf}$ of argon. A standard 230-liter argon dewar (liquid cylinder) typically provides approximately 6000 standard cubic feet (SCF). The gloveroom targets 1000 ppm oxygen, nitrogen, and moisture, rather than glovebox grade impurity levels near $\sim 1\,\mathrm{ppm}$, as the gloveroom is intended only to provide inert secondary containment, not ultra-high purity materials processing.

This constraint can be alleviated by the slow argon displacement technique, with gas inlets placed near the floor so denser argon can slowly and effectively displace air upward toward the exhaust path, reducing total argon usage to several times the volume of gas inside the gloveroom. After the target atmosphere is reached, active PID-controlled circulation can then be initiated and used to homogenize gas composition, improve temperature uniformity, and provide representative analyzer responses. A liquid argon dewar is preferred for extended campaigns because it reduces cylinder changeout burden and better supports slow purge, cover gas operation, and repeated inerting cycles. Moreover, flexible enclosure geometry conforming to the contour of the lithium system using modularized enclosures and compartments can effectively reduce the enclosed volume.

The second limitation is access. Since personnel entry is incompatible with an oxygen-deficient argon atmosphere, maintenance must be planned around purges. The third limitation is scale: increasing the enclosure size would improve access and support taller Phase II open-surface flow geometries, but would also increase purge volume, argon demand, HVAC load, and atmosphere control burden. These limitations motivate the staged LEAP approach, in which Phase I validates enclosed pipe flow, gas handling, monitoring, and thermal management before larger inventory, open surface, and device interface operations are introduced.

6 Summary and conclusions

This work presents a risk-informed design framework for selecting secondary containment architectures for flowing liquid lithium systems. Rather than treating safety and facility complexity as independent objectives, the framework evaluates their qualitative tradeoff through a design penalty index. When applied to representative containment scenarios under PPPL design requirements, the analysis identifies an argon-purged enclosure around an enclosed lithium loop as a favorable architecture for lithium PFC development.

The LEAP case study demonstrates how this tradeoff can be implemented in practice. A modular argon gloveroom provides an inert secondary containment boundary that suppresses the dominant lithium reaction pathways while preserving access, diagnostics, hardware flexibility, and future device interface capability. The architecture also introduces practical constraints, including purge time, argon consumption, oxygen-deficiency controls, and access planning. These costs are acceptable for a staged research platform that must progress from enclosed pipe flow to open-surface lithium PFC testing and eventual fusion-device integration.

Containment architecture should be treated as part of the technology development pathway, not merely as supporting infrastructure. For flowing lithium PFC test systems, a modular inert gloveroom offers a practical middle ground between bench-scale gloveboxes and dedicated lithium facilities. More broadly, the hazard/complexity framework provides a general method for adapting lithium system designs to different inventories, operating modes, facility constraints, and fusion applications. The same logic can also inform other liquid metal systems where safety, maintainability, diagnostics, and rapid iteration must be balanced.

Beyond fusion, liquid-metal systems are used in metallurgy [65], pharmaceuticals [66], soft and flexible electronics [67], and laboratory studies of astrophysical and geophysical magnetohydrodynamics [68–71]. Despite differences in working fluid, temperature, and hazard profile, these systems share a common challenge: reactive, conductive, or high-temperature fluids must be contained without imposing impractical complexity. The containment logic and design penalty index developed here can therefore be adapted to other liquid-metal systems, particularly alkali-metal systems, where chemical reactivity, inerting, diagnostics, and operational access must be balanced.

Acknowledgements

The research described in this paper was conducted under the Laboratory Directed Research and Development (LDRD) Program at Princeton Plasma Physics Laboratory, a national laboratory operated by Princeton University for the U.S. Department of Energy under Prime Contract No. DE-AC02-09CH11466. The United States Government retains a non-exclusive, paid-up, irrevocable, worldwide license to publish or reproduce the published form of this manuscript, or allow others to do so, for United States Government purposes.

The authors thank Richard Majeski, Robert Ellis, Robert Lunsford, Dang Cai, Andrei Khodak, Christian Veyssiere, Andrew Shone, Elise Demoncheaux, Enrique

Miralles-Dolz, the PPPL ESH team, and the LEAP design review committee for fruitful discussions and feedback. The authors thank Rich Cavanaugh, Jiawen Wang, and the rest of the engineering team for LEAP-related design, drawing, and analysis work. The authors thank Creative Engineers, Inc. for comprehensive lithium safety training, which led to many considerations in this work. The authors thank Inert Corp. and MBraun Inc. for providing example product images for the fully-customized and modularized gloveroom.

During the preparation of this work, the authors acknowledge the use of Writefull and ChatGPT (OpenAI) for math and language editing and improving readability. After using this tool/service, the authors reviewed and edited the content as needed and take full responsibility for the content of the publication.

Appendix A Reliability-based interpretation of the mitigation term

The design penalty index used in the main text is intended as a compact downselection metric. A more detailed reliability-based form can be written if component-level mean-time-between-failure (MTBF) data are available. For a component k with MTBF, the corresponding failure frequency is

$$\lambda_k = \frac{1}{\mathrm{MTBF}_k}. \tag{A1}$$

Assuming independent Poisson failures, the probability that component k does not fail during an operating period T is

$$P_{0,k}(T) = \exp(-\lambda_k T). \tag{A2}$$

For hazard mode i, let $\mathcal{K}_i$ denote the set of components that contain the hazard, such as lithium-wetted piping, tanks, or loop components. The probability that at least one of these hazard-containment components fails during T is

$$P_i^{(\mathcal{H})}(T) = 1 - \exp\left[-\sum_{k\in\mathcal{K}_i} \lambda_k^{(\mathcal{H})} T\right]. \tag{A3}$$

Similarly, let $\mathcal{M}_{i,n}$ denote the set of components forming safety layer n for hazard mode i. The probability that safety layer n fails during T is

$$P_{i,n}^{(\mathcal{C})}(T) = 1 - \exp\left[-\sum_{m\in\mathcal{M}_{i,n}} \lambda_m^{(\mathcal{C})} T\right]. \tag{A4}$$

If exposure to hazard mode i requires failure of the hazard containment and simultaneous failure of all relevant safety layers, the residual exposure probability can be

approximated as

$$P_i^{(\mathrm{res})}(T) = P_i^{(\mathcal{H})}(T) \prod_{n \in \mathcal{L}_i} P_{i,n}^{(\mathcal{C})}(T), \tag{A5}$$

where $\mathcal{L}_i$ is the set of safety layers assigned to hazard mode i. A reliability-based design penalty index can then be written as

$$\mathcal{Q}_{\mathrm{rel}} = \alpha \sum_i p_i^{(\mathcal{H})} h_i P_i^{(\mathrm{res})}(T) + \beta \mathcal{C}. \tag{A6}$$

This expression provides a physical interpretation of the residual hazard term in the simplified metric. In particular, eq. (2) may be interpreted as a lumped form in which

$$1 - \gamma_{\mathrm{eff}} \sim P^{(\mathrm{res})}. \tag{A7}$$

In early-stage design, however, the component-level failure frequencies are usually unknown. A reduced heuristic form can be obtained by assuming that the summed hazard-containment failure frequency scales with the hazard index and that the summed safety-layer failure frequency scales with the complexity index,

$$\sum_k \lambda_k^{(\mathcal{H})} T \sim \lambda^{(\mathcal{H})} \mathcal{H} T, \qquad \sum_m \lambda_m^{(\mathcal{C})} T \sim \lambda^{(\mathcal{C})} \mathcal{C} T. \tag{A8}$$

If the number of safety layers also scales with the complexity index, the residual hazard factor can be approximated as

$$P^{(\mathrm{res})} \sim \left[1 - \exp\left(-\lambda^{(H)} \mathcal{H} T\right)\right] \left[1 - \exp\left(-\lambda^{(C)} \mathcal{C} T\right)\right]^{\mathcal{C}}. \tag{A9}$$

This gives the reduced reliability-inspired penalty index

$$\mathcal{Q}_{\mathrm{red}} \sim \alpha \mathcal{H} \left[1 - \exp\left(-\lambda^{(\mathcal{H})} \mathcal{H} T\right)\right] \left[1 - \exp\left(-\lambda^{(\mathcal{C})} \mathcal{C} T\right)\right]^{\mathcal{C}} + \beta \mathcal{C}. \tag{A10}$$

Equation (A10) is not used as the primary scoring method in this work because the lumped failure frequencies and scaling assumptions are not independently known for the candidate architectures. It is nevertheless useful as an interpretation of why an intermediate level of facility complexity can be preferred: additional safety layers reduce residual hazard exposure, but increasing complexity also introduces additional components, interfaces, and failure modes.

Appendix B Optimization of the design penalty index

For convenience, the design penalty indices for different design options are written as

$$\mathcal{Q}(\mathbf{x}) = \alpha \mathcal{H} \left(1 - \gamma_{\mathrm{eff}}(\mathbf{x})\right) + \beta \mathcal{C}(\mathbf{x}), \tag{B11}$$

with

$$\gamma_{\text{eff}}(\mathbf{x}) = \gamma(\mathbf{x}) \exp(-k_H \mathcal{H}(\mathbf{x}) - k_C \mathcal{C}(\mathbf{x})) \,, \tag{B12}$$

and

$$\gamma(\mathbf{x}) = 1 - \exp\left(- \sum_m \eta_m x_m \right). \tag{B13}$$

The optimization problem is

$$\min_{\mathbf{x} \in X} \mathcal{Q}(\mathbf{x}), \tag{B14}$$

where X denotes the set of acceptable design choices.

If the design features are binary (absent/present), $x_m \in \{0, 1\}$, which is suggested in section 2, the problem is not solved by continuous first-order conditions. Instead, the actual optimum is obtained by discrete search, as used in our current study. This search is practical when the number of candidate safety features is modest. However, for the completeness of the problem, we hereby include continuous design features (e.g., argon purge rate, oxygen and moisture set point, spill-capture capacity, redundancy level) and demonstrate a continuous relaxation, which can be useful for ranking feature sensitivity.

B.1 General first-order condition

Let

$$E(\mathbf{x}) = \exp(-k_H \mathcal{H}(\mathbf{x}) - k_C \mathcal{C}(\mathbf{x})) \,, \tag{B15}$$

so that

$$\gamma_{\text{eff}}(\mathbf{x}) = \gamma(\mathbf{x}) E(\mathbf{x}). \tag{B16}$$

Then the design penalty indices become

$$\mathcal{Q}(\mathbf{x}) = \alpha \mathcal{H}(\mathbf{x}) \left(1 - \gamma(\mathbf{x}) E(\mathbf{x})\right) + \beta \mathcal{C}(\mathbf{x}). \tag{B17}$$

Differentiating with respect to a generic and continuous design variable x_m gives

$$\frac{\partial \mathcal{Q}}{\partial x_m} = \alpha \frac{\partial \mathcal{H}}{\partial x_m} \left(1 - \gamma E\right) - \alpha \mathcal{H} \frac{\partial (\gamma E)}{\partial x_m} + \beta \frac{\partial \mathcal{C}}{\partial x_m}. \tag{B18}$$

Applying the product rule,

$$\frac{\partial (\gamma E)}{\partial x_m} = E \frac{\partial \gamma}{\partial x_m} + \gamma \frac{\partial E}{\partial x_m}, \tag{B19}$$

and

$$\frac{\partial E}{\partial x_m} = -E \left(k_H \frac{\partial \mathcal{H}}{\partial x_m} + k_C \frac{\partial \mathcal{C}}{\partial x_m} \right). \tag{B20}$$

Therefore,

$$\frac{\partial (\gamma E)}{\partial x_m} = E \frac{\partial \gamma}{\partial x_m} - \gamma E \left(k_H \frac{\partial \mathcal{H}}{\partial x_m} + k_C \frac{\partial \mathcal{C}}{\partial x_m} \right). \tag{B21}$$

Substituting into eq. (B18) yields

$$\begin{aligned}\frac{\partial \mathcal{Q}}{\partial x_m} &= \alpha \frac{\partial \mathcal{H}}{\partial x_m}(1-\gamma E) - \alpha \mathcal{H} E \frac{\partial \gamma}{\partial x_m} \\ &\quad + \alpha \mathcal{H} \gamma E \left(k_H \frac{\partial \mathcal{H}}{\partial x_m} + k_C \frac{\partial \mathcal{C}}{\partial x_m} \right) + \beta \frac{\partial \mathcal{C}}{\partial x_m}.\end{aligned} \tag{B22}$$

From eq. (B13),

$$\frac{\partial \gamma}{\partial x_m} = \eta_m \exp\left(- \sum_n \eta_n x_n \right) = \eta_m (1-\gamma). \tag{B23}$$

Substituting eq. (B23) into eq. (B22) gives

$$\begin{aligned}\frac{\partial \mathcal{Q}}{\partial x_m} &= \alpha \frac{\partial \mathcal{H}}{\partial x_m}(1-\gamma E) - \alpha \mathcal{H} E\, \eta_m (1-\gamma) \\ &\quad + \alpha \mathcal{H} \gamma E \left(k_H \frac{\partial \mathcal{H}}{\partial x_m} + k_C \frac{\partial \mathcal{C}}{\partial x_m} \right) + \beta \frac{\partial \mathcal{C}}{\partial x_m}.\end{aligned} \tag{B24}$$

An interior optimum $\mathbf{x}^*$ must satisfy

$$\left. \frac{\partial \mathcal{Q}}{\partial x_m} \right|_{\mathbf{x}^*} = 0 \qquad \text{for all } m. \tag{B25}$$

B.2 Special case: fixed $\mathcal{H}$, linear $\mathcal{C}$

A practically useful simplification is to treat the intrinsic hazard level as fixed for a given experiment class,

$$\mathcal{H}(\mathbf{x}) = \mathcal{H}_0, \qquad \frac{\partial \mathcal{H}}{\partial x_m} = 0, \tag{B26}$$

and to model the complexity as a weighted linear sum,

$$\mathcal{C}(\mathbf{x}) = \sum_m c_m x_m, \qquad \frac{\partial \mathcal{C}}{\partial x_m} = c_m. \tag{B27}$$

Then eq. (B24) reduces to

$$\frac{\partial \mathcal{Q}}{\partial x_m} = -\alpha \mathcal{H}_0 E\, \eta_m (1-\gamma) + \alpha \mathcal{H}_0 \gamma E\, k_C c_m + \beta c_m, \tag{B28}$$

where

$$E = \exp(-k_H \mathcal{H}_0 - k_C \mathcal{C}(\mathbf{x}))\,. \tag{B29}$$

This derivative indicates whether increasing the extent or strength of the mitigation feature m would reduce the penalty in the continuous relaxation of the problem. Thus, the first-order condition becomes

$$-\alpha \mathcal{H}_0 E\, \eta_m (1-\gamma) + \alpha \mathcal{H}_0 \gamma E\, k_C c_m + \beta c_m = 0. \tag{B30}$$

The first term represents the hazard-reduction benefit of adding the feature m and is largest when the intrinsic hazard is high, and the current mitigation level is still limited. The second term is complexity-induced degradation of effectiveness. The third term is the direct complexity penalty. This last penalty is independent of hazard reduction physics. It simply reflects that complex systems are harder and more expensive to build and run.

Equation (B30) has a clear interpretation: a safety feature should be included only up to the point where its reduction of residual hazard is matched by the added penalty from increased facility complexity and from the loss of practical effectiveness caused by that extra complexity.

References

[1] Müller, U., Bühler, L.: Magnetofluiddynamics in Channels and Containers. Springer, Berlin (2001)

[2] Davidson, P.A.: Introduction to Magnetohydrodynamics. Cambridge University Press, Cambridge (2017)

[3] Tang, S.-Y., Tabor, C., Kalantar-Zadeh, K., Dickey, M.D.: Gallium liquid metal: the devil's elixir. Annual Review of Materials Research **51**(1), 381–408 (2021)

[4] Coenen, J., De Temmerman, G., Federici, G., Philipps, V., Sergienko, G., Strohmayer, G., Terra, A., Unterberg, B., Wegener, T., Bekerom, D.: Liquid metals as alternative solution for the power exhaust of future fusion devices: status and perspective. Physica Scripta **159**(1), 014037 (2014)

[5] Ono, M., Majeski, R., Jaworski, M.A., Hirooka, Y., Kaita, R., Gray, T.K., Maingi, R., Skinner, C.H., Christenson, M., Ruzic, D.N.: Liquid lithium loop system to solve challenging technology issues for fusion power plant. Nuclear Fusion **57**(11), 116056 (2017)

[6] Kaita, R.: Fusion applications for lithium: wall conditioning in magnetic confinement devices. Plasma Physics and Controlled Fusion **61**(11), 113001 (2019)

[7] De Castro, A., Moynihan, C., Stemmley, S., Szott, M., Ruzic, D.: Lithium, a path to make fusion energy affordable. Physics of Plasmas **28**(5) (2021)

[8] Urgorri, F.R., Smolentsev, S., Fernández-Berceruelo, I., Rapisarda, D., Palermo, I., Ibarra, A.: Magnetohydrodynamic and thermal analysis of pbli flows in poloidal channels with flow channel insert for the eu-dcll blanket. Nuclear Fusion **58**(10), 106001 (2018)

[9] U.S. Department of Energy: Fusion science & technology roadmap. Technical report, U.S. Department of Energy (2026). https://www.energy.gov/documents/fusion-st-roadmap-060926pdf

[10] Golubchikov, L., Evtikhin, V., Lyublinski, I., Pistunovich, V., Potapov, I., Chumanov, A.: Development of a liquid-metal fusion reactor divertor with a capillary-pore system. Journal of Nuclear Materials **233**, 667–672 (1996)

[11] Mirnov, S., Lazarev, V., Sotnikov, S., Evtikhin, V., Lyublinski, I., Vertkov, A., *et al.*: Li-cps limiter in tokamak t-11m. Fusion Engineering and Design **65**(3), 455–465 (2003)

[12] Herrmann, A., Greuner, H., Jaksic, N., Balden, M., Kallenbach, A., Krieger, K., De Marné, P., Rohde, V., Scarabosio, A., Schall, G., *et al.*: Solid tungsten divertor-iii for asdex upgrade and contributions to iter. Nuclear Fusion **55**(6), 063015 (2015)

[13] Nygren, R.E., Rudakov, D.L., Murphy, C., Watkins, J.D., Unterberg, E.A., Barton, J.L., Stangeby, P.C.: Thermal management of tungsten leading edges in diii-d. Fusion Engineering and Design **124**, 271–275 (2017)

[14] Pitts, R., Bardin, S., Bazylev, B., Van Den Berg, M., Bunting, P., Carpentier-Chouchana, S., Coenen, J., Corre, Y., Dejarnac, R., Escourbiac, F., *et al.*: Physics conclusions in support of iter w divertor monoblock shaping. Nuclear Materials and Energy **12**, 60–74 (2017)

[15] Sinclair, G., Tripathi, J., Diwakar, P., Hassanein, A.: Melt layer erosion during elm-like heat loading on molybdenum as an alternative plasma-facing material. Scientific reports **7**(1), 12273 (2017)

[16] Wang, S., Li, J., Wang, Y., Zhang, X., Wang, R., Wang, Y., Cao, J.: Thermal damage of tungsten-armored plasma-facing components under high heat flux loads. Scientific Reports **10**(1), 1359 (2020)

[17] Fisher, A., Sun, Z., Kolemen, E.: Liquid metal "divertorlets" concept for fusion reactors. Nuclear Materials and Energy **25**, 100855 (2020)

[18] Saenz, F., Sun, Z., Fisher, A.E., Wynne, B., Kolemen, E.: Divertorlets concept for low-recycling fusion reactor divertor: experimental, analytical and numerical verification. Nuclear Fusion **62**(8), 086008 (2022)

[19] Morley, N.B., Abdou, M.A.: Modeling of fully-developed, liquid metal, thin film flows for fusion divertor applications. Fusion engineering and design **30**(4), 339–356 (1995)

[20] Pan, J.-H., Ni, M.-J.: Magnetohydrodynamic effects on liquid metal flows in an open channel for fusion plasma facing components with a transverse magnetic field. Nuclear Fusion **65**(4), 046015 (2025)

[21] Jiang, Y., Aduloju, S., Smolentsev, S.: Design and analysis of the open-surface slow li flow divertor and comparison to the fast li flow divertor. Fusion Science

and Technology **82**(1-2), 135–155 (2026)

[22] Khodak, A., Maingi, R.: Plasma facing components with capillary porous system and liquid metal coolant flow. Physics of Plasmas **29**(7) (2022)

[23] Ruzic, D., Xu, W., Andruczyk, D., Jaworski, M.: Lithium–metal infused trenches (limit) for heat removal in fusion devices. Nuclear Fusion **51**(10), 102002 (2011)

[24] Goldston, R.J., Myers, R., Schwartz, J.: The lithium vapor box divertor. Physica Scripta **167**(1), 014017 (2016)

[25] Emdee, E., Goldston, R.J., Schwartz, J., Rensink, M., Rognlien, T.: A simplified lithium vapor box divertor. Nuclear Fusion **59**(8), 086043 (2019)

[26] Ruzic, D., Szott, M., Sandoval, C., Christenson, M., Fiflis, P., Hammouti, S., Kalathiparambil, K., Shchelkanov, I., Andruczyk, D., Stubbers, R., *et al.*: Flowing liquid lithium plasma-facing components–physics, technology and system analysis of the limit system. Nuclear Materials and Energy **12**, 1324–1329 (2017)

[27] Islam, M.S., Lore, J.D., Smolentsev, S., Kessel, C.E., Maingi, R.: Analysis and design of fast flow liquid li divertor for fusion nuclear science facility (fnsf) using coupled plasma boundary and lm mhd/heat transfer codes. Nuclear Fusion **64**(5), 056036 (2024)

[28] Kuang, A., Ballinger, S., Brunner, D., Canik, J., Creely, A., Gray, T., Greenwald, M., Hughes, J., Irby, J., LaBombard, B., *et al.*: Divertor heat flux challenge and mitigation in sparc. Journal of Plasma Physics **86**(5), 865860505 (2020)

[29] Coburn, J., Effenberg, F., Cusentino, M.A., Hargrove, C., Ialovega, M., Morbey, M., Nuckols, L., Popović, Ž., Bergstrom, Z., Zamperini, S., et al.: Overview of advanced plasma-facing materials testing for fusion pilot plants at diii-d. Nuclear Materials and Energy, 102064 (2026)

[30] Majeski, R., Doerner, R., Gray, T., Kaita, R., Maingi, R., Mansfield, D., Spaleta, J., Soukhanovskii, V., Timberlake, J., Zakharov, L.: Enhanced energy confinement and performance in a low-recycling tokamak. Physical Review Letters **97**(7), 075002 (2006)

[31] Boyle, D.P., Anderson, J., Banerjee, S., Bell, R., Capecchi, W., Elliott, D., Hansen, C., Kubota, S., LeBlanc, B., Maan, A., *et al.*: Extending the low-recycling, flat temperature profile regime in the lithium tokamak experiment-β (ltx-β) with ohmic and neutral beam heating. Nuclear Fusion **63**(5), 056020 (2023)

[32] Kugel, H., Allain, J., Bell, M., Bell, R., Diallo, A., Ellis, R., Gerhardt, S., Heim, B., Jaworski, M., Kaita, R., *et al.*: Nstx plasma operation with a liquid lithium divertor. Fusion Engineering and Design **87**(10), 1724–1731 (2012)

[33] Mazzitelli, G., Apicella, M., Frigione, D., Maddaluno, G., Marinucci, M., Mazzotta, C., Pericoli Ridolfini, V., Romanelli, M., Szepesi, G., Tudisco, O., *et al.*: Ftu results with a liquid lithium limiter. Nuclear Fusion **51**(7), 073006 (2011)

[34] Tabarés, F., Ochando, M., Medina, F., Tafalla, D., Ferreira, J., Ascasibar, E., Balbín, R., Estrada, T., Fuentes, C., García-Cortés, I., *et al.*: Plasma performance and confinement in the tj-ii stellarator with lithium-coated walls. Plasma Physics and Controlled Fusion **50**(12), 124051 (2008)

[35] Zuo, G., Hu, J., Li, J., Luo, N., Zakharov, L., Zhang, L., Ti, A.: First results of lithium experiments on east and ht-7. Journal of Nuclear Materials **415**(1), 1062–1066 (2011)

[36] Maingi, R., Osborne, T., LeBlanc, B., Bell, R., Manickam, J., Snyder, P., Menard, J., Mansfield, D., Kugel, H., Kaita, R., *et al.*: Edge-localized-mode suppression through density-profile modification with lithium-wall coatings in the national spherical torus experiment. Physical Review Letters **103**(7), 075001 (2009)

[37] Zuo, G., Hu, J., Li, J., Sun, Z., Mansfield, D., Zakharov, L.: Lithium coating for h-mode and high performance plasmas on east in asipp. Journal of Nuclear Materials **438**, 90–95 (2013)

[38] Gupta, D., Brooks, A., Brown, T., Khodak, A., Linn, B., Menard, J.: Mhd analysis of dual-coolant lead-lithium blanket for spherical tokamak advanced reactor. Fusion Science and Technology **82**(1-2), 252–273 (2026)

[39] Abdou, M., Riva, M., Ying, A., Day, C., Loarte, A., Baylor, L., Humrickhouse, P., Fuerst, T.F., Cho, S.: Physics and technology considerations for the deuterium–tritium fuel cycle and conditions for tritium fuel self sufficiency. Nuclear Fusion **61**(1), 013001 (2021)

[40] Sawan, M., Abdou, M.: Physics and technology conditions for attaining tritium self-sufficiency for the dt fuel cycle. Fusion Engineering and Design **81**(8-14), 1131–1144 (2006)

[41] Baus, C., Barron, P., D'Angiò, A., Hirata, Y., Konishi, S., Mund, J., Nagao, T., Nakahara, D., Pearson, R., Sakaguchi, M., *et al.*: Kyoto fusioneering's mission to accelerate fusion energy: Technologies, challenges and role in industrialisation. Journal of Fusion Energy **42**(1), 10 (2023)

[42] Bohm, T.D., Davis, A., Harb, M.S., Marriott, E.P., Wilson, P.P.: Initial neutronics investigation of a liquid-metal plasma-facing fusion nuclear science facility. Fusion Science and Technology **75**(6), 429–437 (2019)

[43] Lane, J.A., MacPherson, H.G., Maslan, F.: Fluid Fuel Reactors: Molten Salt Reactors, Aqueous Homogeneous Reactors, Fluoride Reactors, Chloride Reactors, Liquid Metal Reactors and Why Liquid Fission. Addison-Wesley Pub. Co.,

Reading (1958)

[44] Michal, R.: Fifty years ago in december: Atomic reactor ebr-i produced first electricity. Nuclear News **44**(12), 28–29 (2001)

[45] Kultgen, D., Weathered, M., Kent, E., Rein, J., Grannan, A., Grandy, C.: Mechanisms engineering test loop (metl) operations and testing report (fy2022). Technical report, Argonne National Laboratory (ANL), Argonne, IL (United States) (2022)

[46] Generation IV International Forum: Sodium Fast Reactor (SFR). https://www.gen-4.org/generation-iv-criteria-and-technologies/sodium-fast-reactor-sfr. Accessed 2026-05-02 (n.d.)

[47] Marshall, A.C.: An assessment of reactor types for thermochemical hydrogen production. Technical Report SAND2002-0513, Sandia National Laboratories (February 2002). https://www.osti.gov/servlets/purl/793338

[48] Jackson, C.B.e..: Liquid metals handbook: Sodium-nak supplement. Technical Report TID-5277, Atomic Energy Commission; Bureau of Ships (July 1955). https://www.osti.gov/biblio/4376530

[49] Foust, O.J.: Sodium-NaK Engineering Handbook. Volume III: Sodium Systems, Safety, Handling, and Instrumentation. [LMFBR]. Gordon and Breach, Science Publishers, Inc., New York (1978). https://www.osti.gov/biblio/6639472

[50] Miyakawa, A., Maeda, H., Kani, Y., Ito, K.: Sodium leakage experience at the prototype fbr monju. IAEA. (2000)

[51] Hvasta, M., Kent, E., Kultgen, D., Rein, J., Weathered, M., Grannan, A., Ogren, E., Grandy, C.: Mechanisms engineering test loop (metl) experimenter's guide-revision 2. Technical report, Argonne National Laboratory (ANL), Argonne, IL (United States) (2024)

[52] D'Ovidio, G., Martín-Fuertes, F., Marugán, J.C., Bermejo, S., Nitti, F.S.: Lithium fire protection design approach in ifmif-dones facility. Fusion Engineering and Design **189**, 113446 (2023)

[53] Maroni, V., Beatty, R., Brown, H., Coleman, L., Foose, R., McPheeters, C., Slawecki, M., Smith, D., Van Deventer, E., Weston, J.: Analysis of the october 5, 1979 lithium spill and fire in the lithium processing test loop. Technical report, Argonne National Lab., IL (USA) (1981)

[54] Nygren, R.: Sandia plasma materials test facility (pmtf) and actions after li fire on 26 aug 2011. Technical report/presentation, Sandia National Laboratories (2012)

[55] Pérez, M., D'Ovidio, G., Martin-Fuertes, F.: Application of the melcor for fusion

code to the transient accident analysis of the ifmif-dones test cell. Journal of Fusion Energy **42**(2), 38 (2023)

[56] International Code Council: 2021 International Building Code, Washington, DC. Section 307, Hazardous Materials (2021). https://codes.iccsafe.org/s/IBC2021P1/chapter-3-occupancy-classification-and-use/IBC2021P1-Ch03-Sec307.8

[57] National Fire Protection Association: NFPA 484: Standard for Combustible Metals, Quincy, MA (2022). https://www.nfpa.org/product/nfpa-484-standard/p0484code

[58] International Code Council: 2024 International Fire Code, Washington, DC (2024). https://codes.iccsafe.org/content/IFC2024P1

[59] International Atomic Energy Agency: Fire Protection in Nuclear Power Plants, Vienna (2021). https://www.iaea.org/publications/14797/fire-protection-in-nuclear-power-plants

[60] The American Society of Mechanical Engineers: ASME B31.3: Process Piping, New York, NY (2024). https://www.asme.org/codes-standards/find-codes-standards/b313-2018-process-piping

[61] The American Society of Mechanical Engineers: ASME Boiler and Pressure Vessel Code, New York, NY (2025). https://www.asme.org/codes-standards/bpvc-standards/bpvc-2025

[62] Gertman, D., Blackman, H., Marble, J., Byers, J., Smith, C., *et al.*: The spar-h human reliability analysis method. US Nuclear Regulatory Commission **230**(4), 35 (2005)

[63] Bernoulli, D.: Exposition of a new theory on the measurement of risk. In: The Kelly Capital Growth Investment Criterion: Theory and Practice, pp. 11–24. World Scientific, Singapore (2011)

[64] Kinsley Jr, G.R.: Properly purge and inert storage vessels. Natural gas (Pittsburgh) **12**, 14–5 (2001)

[65] Wei, S., Lampman, S.: Centrifugal casting. In: Casting, pp. 667–673. ASM International, Materials Park (2008)

[66] Wang, Q., Yu, Y., Liu, J.: Preparations, characteristics and applications of the functional liquid metal materials. Advanced Engineering Materials **20**(5), 1700781 (2018)

[67] Dickey, M.D.: Stretchable and soft electronics using liquid metals. Advanced materials **29**(27), 1606425 (2017)

[68] Adams, M.M., Stone, D.R., Zimmerman, D.S., Lathrop, D.P.: Liquid sodium models of the earth's core. Progress in Earth and Planetary Science **2**(1), 29 (2015)

[69] Stefani, F., Gailitis, A., Gerbeth, G., Giesecke, A., Gundrum, T., Rüdiger, G., Seilmayer, M., Vogt, T.: The dresdyn project: liquid metal experiments on dynamo action and magnetorotational instability. Geophysical & Astrophysical Fluid Dynamics **113**(1-2), 51–70 (2019)

[70] Xu, Y., Horn, S., Aurnou, J.M.: Thermoelectric precession in turbulent magnetoconvection. Journal of Fluid Mechanics **930**, 8 (2022)

[71] Liu, T., Xu, Y., Abbate, J.A., Cheng, J.S., Aurnou, J.M.: Geostrophic to magnetically-damped turbulence in liquid metal rotating magnetoconvection. Physics of the Earth and Planetary Interiors **374**, 107535 (2026) https://doi.org/10.1016/j.pepi.2026.107535